Engineering Structures 335 (2025) 120347

Contents lists available at ScienceDirect

Engineering Structures

journal homepage: www.elsevier.com/locate/engstruct

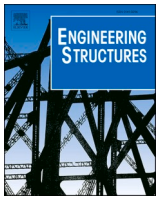

Probabilistic assessment of seismic acceleration demands of ductile light NSCs in moderately ductile RC frame buildings

Majid Mehrjoo *, Rola Assi

Department of construction engineering, École de technologie supérieure (ÉTS), Montreal, Quebec H3C 1K3, Canada

ARTICLE INFO

Keywords:
Non-structural components
Ductile behavior
Component attachments
Iterative Newmark integration
Dynamic analysis
Peak component accelerations

ABSTRACT

This study investigates how the seismic demands of non-structural components (NSCs) are influenced by both their attachment ductility and the nonlinear behavior of supporting structures. The research focuses on acceleration demands at various building elevations and evaluates component damage states according to Hazus guidelines. Incremental dynamic analysis (IDA) was applied to evaluate both linear and nonlinear structural responses of four archetype reinforced concrete moment-resisting frame buildings. Ground motions, consisting of historical and synthetic records, were scaled to match Montreal's uniform hazard spectrum for Site Class 'C' with a 2 % probability of exceedance per 50 years. NSC responses were assessed using an uncoupled analysis approach, implemented through iterative Newmark integration. Key findings demonstrate that increasing the ductility of NSC attachments reduces their acceleration demands by up to 140 % in elastic structures. When accounting for structural nonlinearity, acceleration demands decrease by 110 %, highlighting the conservative nature of elastic analysis assumptions commonly used in current design practices. These reductions are most pronounced for components with periods corresponding to the structure's fundamental mode, with the effect diminishing for higher modes. The research provides practical design implications by quantifying the relationship between attachment ductility, structural behavior, and component damage thresholds. The results indicate that a moderately ductile ($\mu \approx 1.5$) NSC attachment provides optimal performance benefits while minimizing the risk of NSC damage, offering valuable insights for the performance-based design of NSCs.

1. Introduction

This study provides a comprehensive probabilistic examination of the impact of the extent of ductility of attachment of acceleration-sensitive non-structural components (NSCs) on their seismic demands. Examples of such NSCs include water heaters, chillers, antennas, chimneys, and parapets [1–6]. Accurate evaluation of these acceleration demands is critical for the design, performance, and fragility analysis of these NSCs [7,8].

Research has shown that the ductility of NSCs' attachments plays a crucial role in reducing seismic demands, particularly within the resonance range of a building's fundamental period [5,9–12]. Various numerical approaches have been employed to investigate the impact of the ductile behavior of NSCs attachments on their seismic demands. These approaches may be generally categorized into three main types: advanced numerical simulations, simplified analytical techniques, and empirical code-based procedures.

Advanced numerical approaches that integrate seismic probabilistic assessment methods are necessary for a more comprehensive and accurate evaluation of NSCs' seismic demands. In this context, two prominent methodologies stand out: Incremental Dynamic Analysis (IDA) and Multiple-Stripe Analysis (MSA). IDA provides a comprehensive simulation framework to assess seismic demands across a continuous range of earthquake intensities by applying scaled accelerograms to the building model. MSA offers a complementary approach by analyzing structural response at discrete intensity levels using ground motion sets specifically selected for each intensity level [13]. In this study, IDA was selected as it enables the generation of continuous fragility curves to evaluate component performance corresponding to different damage states [14–16]. On the other hand, simplified analytical techniques such as the nonlinear static analysis or the floor response spectra (FRS) are used to provide a preliminary assessment of the influence of the ductility of attachment of NSCs on the seismic demands of these components [17]. On the other hand, these techniques have limitations in capturing the nonlinear responses of structures and NSCs because of the oversimplification of complex behaviors such as material

* Corresponding author.
E-mail addresses: majid.mehrjoo.1@ens.etsmtl.ca (M. Mehrjoo), rola.assi@etsmtl.ca (R. Assi).

https://doi.org/10.1016/j.engstruct.2025.120347
Received 31 August 2024; Received in revised form 9 April 2025; Accepted 13 April 2025
Available online 21 April 2025

nonlinearity of the structural components and the ductile behavior of NSC attachments, which creates challenges in accounting for cumulative damage effects and may result in an overestimation of seismic demands [18–21]. Additionally, empirical methods, which form the basis of most seismic design codes, tend to use simplified equations and assumptions to estimate the seismic demands on NSCs [4,22]. Specifically, the National Building Code of Canada (NBC) suggests a force-based approach for the design of NSCs, incorporating parameters such as the component response modification factor (Rp) to account for the ductility at NSC's attachment [23]. Specifically, current analytical approaches in NBC provision primarily focus on the elastic behavior of the NSCs and the supporting structure, thereby potentially overestimating seismic demands [24–27]. Despite their usefulness in simplifying the design procedures, empirical methods require improvement to more accurately represent the level of ductility of NSCs' attachment [4,5,22,28–32].

To address the nonlinear behavior of NSCs and their supporting structures, advanced analytical approaches have been employed to overcome the limitations of code-simplified methods. Notably, studies by Lin and Mahin [26] and Taghavi and Miranda [33] demonstrated that inelastic structural responses can either amplify or attenuate floor accelerations compared to linear models, depending on factors such as building height, lateral system flexibility, and NSC period. Recent work by Ruggieri and Vukobratović [34] also emphasizes that accounting for nonlinear behavior can reduce acceleration demands by up to 40 %, compared to elastic analysis predictions, particularly when considering energy dissipation through structural ductility and irregularities in mass and stiffness. Clayton and Medina [35] proposed a probabilistic method to estimate acceleration demands for NSCs in shear wall structures based on the three NSCs (T_C) period ranges, rigid region ($T_C \rightarrow 0$), short-period region ($0 < T_C < 0.5\ T_{B1}$), and fundamental-period region ($0.5\ T_{B1} < T_C < 2.0\ T_{B1}$). IDA and site-specific ground-motion hazard data were used to develop hazard curves and component uniform hazard spectra (CUHS) considering various structural and NSC characteristics. The study found that component location, period ratios, and damping ratios are critical factors in estimating component responses.

Another key aspect in understanding NSC behavior is their fragility response to seismic loads. In this context, D'Angela et al. [36] conducted a comprehensive study of the seismic fragility of NSCs modeled as nonlinear single-degree-of-freedom systems. The research utilized IDA to evaluate the seismic response of a range of NSC frequencies, including medical equipment, suspended ceiling systems, and museum objects. The various damage states and performance levels for each NSC category were evaluated in the analysis, which resulted in the production of fragility curves that are valuable in the seismic design and vulnerability assessment of NSCs. The results showed that as the rigidity of the NSCs increased, the probability of exceeding damage states tended to decrease. Conversely, fragility dispersion exhibited the opposite trend, which will decrease as the rigidity of NSCs increases. Gautam et al. [37] investigated the seismic fragility of structural and NSCs in RC buildings in Nepal, using detailed vulnerability assessments of school buildings after the 2015 Gorkha Earthquake (M_w 7.8). This assessment provides insights into their seismic demands and highlights the urgent need for strengthening the NSCs and beam-column connections.

While previous research has established the importance of NSC seismic behavior and provided valuable insights into their performance under different levels of ground motion intensity and structural configurations, there remains a critical need to understand the combined effects of NSC attachment ductility and structural nonlinearity on component seismic demands and damage states. Additionally, while the impact of structural ductility on seismic response has been well-documented, the relationship between NSC attachment ductility and acceleration demands across different floor levels and damage states remains insufficiently explored [38–40].

To address the existing knowledge gaps, this research focuses on three key objectives: (1) quantifying the relationship between NSC attachment ductility and seismic demands through probabilistic assessment, (2) evaluating the combined influence of structural nonlinearity and NSC ductility on component acceleration demands, and (3) developing practical design recommendations for optimal NSC attachment ductility levels that balance performance and damage control to support performance-based design of NSC attachments. To achieve these goals, this study employs IDA to evaluate the seismic demands of acceleration-sensitive NSCs and develop fragility curves. The analysis is based on three elevation levels along the building height (roof, intermediate, and ground) for four multi-story archetype reinforced concrete moment-resisting frame buildings subjected to 24 earthquake records matching Montreal's uniform hazard spectrum (UHS). Advanced numerical approaches were used to establish a correlation between four ductility levels and the damage states, slight, moderate, and extensive, specified in the Hazus manual [41]. The use of the Hazus classification approach provides a foundation for a broader analysis of NSCs while recognizing the inherent limitations of creating specific fragility curves for all component types in different regions [41]. The methodology employs multi-degree-of-freedom (MDOF) vibration systems in both elastic and elasto-plastic archetype-building models. Elasto-plastic behavior is used as a simplifying assumption to capture the essential nonlinear characteristics of the building while maintaining computational efficiency [9,42,43]. This analysis considers the NSCs with periods that match the first three periods for each case study building.

2. Selection and scaling of input ground motion data

This study employs a total of 24 ground motion recordings, which include a suite of 12 historical ground motions and 12 synthetic ground motions, to accurately estimate the mean structural response quantities [44,45]. The selected ground motions are representative of Montreal's seismic hazard characteristics, characterized by low-to-moderate seismicity. Historical ground motions were chosen to reflect regional tectonic settings, while synthetic motions were included to account for scenarios that may not be adequately represented in the historical dataset. This approach ensures comprehensive coverage of potential seismic hazards while maintaining consistency with Montreal's UHS [46]. It is acknowledged, however, that synthetic records may exhibit certain properties, such as increased energy content or a higher number of cycles, potentially influencing the seismic demands on structures [47]. To address this, frequency domain matching [48] was employed through a MATLAB script to match synthetic and historical earthquakes with Montreal's target UHS for Site Class 'C', based on a 2 % probability of exceedance in 50 years and a damping ratio of 5 %. This Frequency domain matching involves defining the response spectra for the given accelerogram, defining the modification factors, and applying the frequency domain amplitude correction through the Fast Fourier Transform (FFT) algorithm to minimize the disparities in the spectral values. An inverse FFT is then performed to obtain the scaled time history records.

This technique preserves the inherent features of seismic ground motions while ensuring that the energy distribution and spectral characteristics of the records are consistent with the target design spectrum, thereby minimizing potential biases in seismic demand estimation [49]. While this study's methodology focused on Montreal's Site Class 'C', it can be extended to other site classes and regions with varying seismic hazard zones. Such applications would broaden the scope of the research and enhance the understanding of NSC ductile behavior and seismic demands under a broader range of seismic conditions.

a) Historical ground motions

A collection of 12 far-field ground motions from the PEER NGA-East database was chosen, as shown in Table 1 and Fig. 1, based on the following criteria [23,50,51]:

Table 1
Details of selected historical ground motions.

No	Event/Station	Date/Time	Mw
1	Saguenay/Site 2, Quebec, PQ	1988–11–25	5.9
2	FtPayne_2003–04–29/Sewanee	2003–04–29 8:59	4.62
3	MtCarmel_2008–04–18a/Olney Central College Olney, IL	2008–04–18 15:14	4.64
4	MtCarmel_2008–04–18a/Univ. of Southern Indiana, Evansville, IN	2008–04–18 15:14	4.64
5	Slaughterville_2010–10–13/Jones High School	2010–10–13 14:06	4.36
6	Slaughterville_2010–10–13/Wilshire Boulevard- Harrah	2010–10–13 14:06	4.36
7	Arcadia_2010–11–24/Meyer Ranch, Chandler, OK	2010–11–24 22:48	3.96
8	Arcadia_2010–11–24/Bridge Creek, Tuttle, OK	2010–11–24 22:48	3.96
9	Sparks_2011–11–05/Pawnee, OK	2011–11–05 7:12	4.73
10	Sparks_2011–11–05/Meyer Ranch, Chandler, OK	2011–11–05 7:12	4.73
11	Sparks_2011–11–06/Jones High School	2011–11–06 3:53	5.68
12	Sparks_2011–11–06/Wilshire Boulevard-Harrah	2011–11–06 3:53	5.68

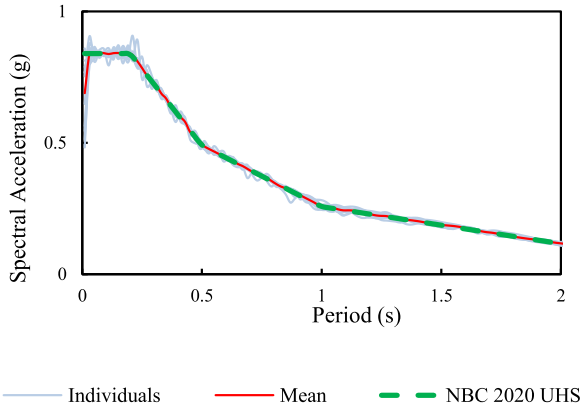

Fig. 1. Mean and individual spectra of scaled historical ground motion and NBC 2020 UHS with a 2 % possibility of exceedance per 50 years in Montreal.

1. Moderate earthquake magnitudes (Mw) were considered, ranging from 3.5 to 6.
2. Far-field records, which dominate Montreal's seismic environment [52,53] were chosen with epicentral distances ranging between 20 and 100 km
3. The strike-slip fault mechanism was selected [54].
4. Average shear-wave velocities in the range of 360–760 cm/sec in the top 30 m of soil (Vs-30) were chosen to represent very dense soil known as Site Class 'C' in the NBC 2020.

b) Synthetic ground motions

A collection of 12 synthetic accelerograms was extracted from the database developed by Atkinson [55] and made available through the Engineering Seismology Toolbox website (www.seismotoolbox.ca). For the selection process, six records were considered for each magnitude-distance (M-R) scenario and were subsequently scaled to be compatible with Montreal UHS for Site class 'C' with a 2475-year return period. The properties of the selected accelerograms are detailed in Table 2, and their response spectra, along with Montreal's UHS, are depicted in Fig. 2.

Table 2
Details of the synthetic ground motions.

M_w	R	Record	Duration(s)	Time step(s)	PGA(g)
6.0	15	E6c1_43	43.598	0.002	0.607
		E6c1_4			0.368
		E6c1_21			0.493
	30	E6c2_17	47.530		0.522
		E6c2_37			0.419
		E6c2_15			0.338
7.0	25	E7c1_18	51.126	0.002	0.395
		E7c1_30			0.285
		E7c1_40			0.538
	100	E7c2_12	57.352		0.213
		E7c2_4			0.329
		E7c2_36			0.178

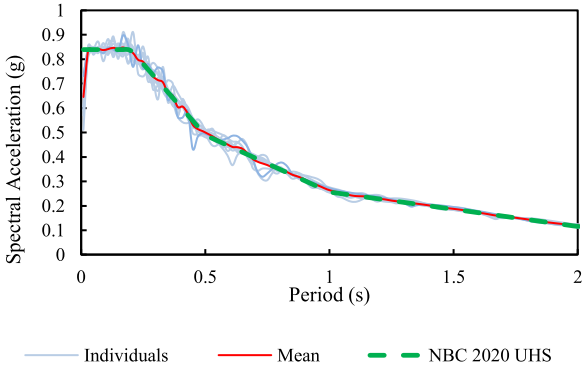

Fig. 2. Mean, individual spectra of scaled synthetic records, and NBC 2020 UHS with 2 % possibility of exceedance per 50 years in Montreal.

3. Description of the case study buildings and their modeling assumptions

The present investigation focused on a set of symmetric and regular 3-, 6-, 9-, and 12-story reinforced concrete (RC) moment-resisting frame (MRF) structures with limited ductility and a normal importance category. The buildings share a common layout, consisting of three bays, each spanning 7 m in both the north-south (N-S) and east-west (E-W) directions, with a standard floor height of 3 m, as shown in Fig. 3. The structures were designed following the guidelines specified in NBC 2015 [56] and CSA A23.3–14 [57], with the design details addressed in the research of Mazloom and Assi [58]. The fundamental periods for these case studies are shown in Table 3.

The buildings were represented by stick models with lumped mass and stiffness at each floor, enabling the creation of matrices to analyze the MDOF system with 5 % modal damping.

The stiffness of each level of the buildings modeled in the ETABS software [59] was determined using the flexibility method, which involves applying a unit force to each degree of freedom individually, calculating the resulting displacements, assembling these displacements into a flexibility matrix, and finally obtaining the stiffness matrix by inverting the flexibility matrix [60,61].

In order to determine the building's nonlinear floor acceleration responses, the governing equations of motion were solved using the Newmark integration technique.

The method was implemented in a MATLAB [62] script, using the yield displacement of each floor derived from pushover analysis, which provides insight into structural nonlinear behavior. In order to perform the pushover analysis in ETABS, concentrated plastic hinges were used to represent material nonlinearity at specific points in beams and columns, following the acceptance criteria outlined in ASCE 41–17 [32]. The nonlinear behavior characterization of these plastic hinges follows a standardized force-deformation relationship, as illustrated in Fig. 4,

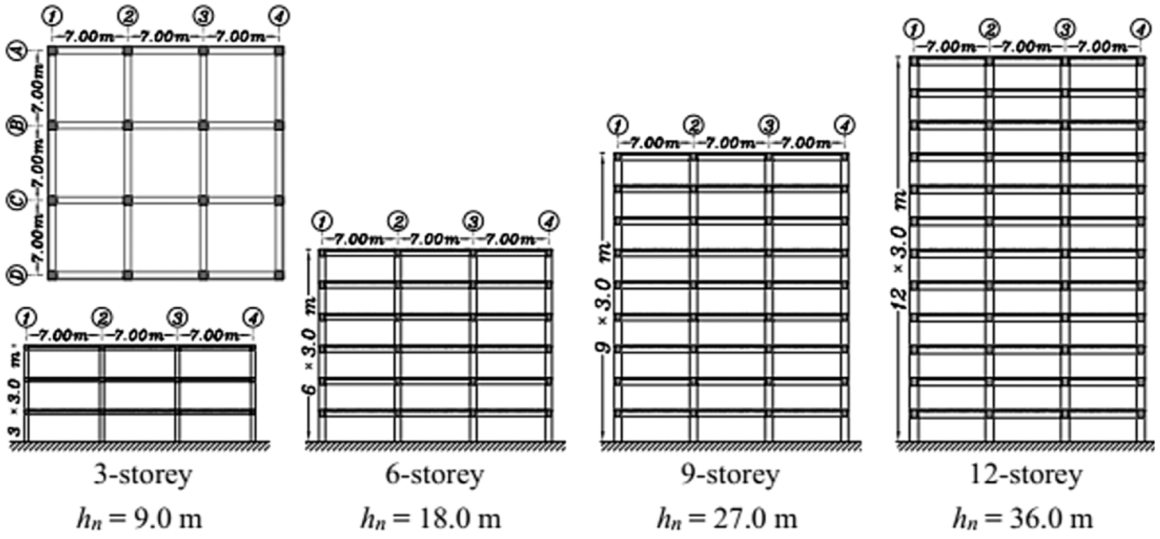

Fig. 3. Plan and elevation views of the archetype reinforced concrete moment-resisting frame buildings used in this research [63].

Table 3
The first three periods of the case study buildings.

Case study	T_1 (s)	T_2(s)	T_3(s)
3 Storey	0.973	0.279	0.182
6 Storey	1.014	0.321	0.189
9 Storey	1.354	0.441	0.261
12 Storey	1.468	0.279	0.182

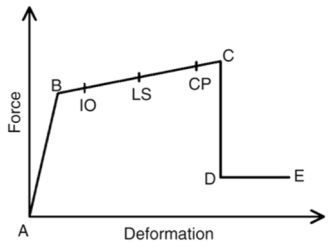

Fig. 4. Force–deformation relationship of a typical plastic hinge.

where key behavioral points denote: 'a' (effective yield), 'b' (peak strength), and 'c' (residual strength). The analysis incorporates three critical performance levels: IO (Immediate Occupancy), LS (Life Safety), and CP (Collapse Prevention), which define the progressive degradation of structural capacity. Based on this behavioral framework, two-moment plastic hinges were assigned near the rigid zones at the ends of element, allowing for plastic hinge formation close to the joint faces. The beams were modeled with pure bending hinges while column hinges were modeled with axial force-bending moment interaction as introduced in Table A.1. The analyses continued until the displacement of the roof matched the predetermined target displacement, calculated using Eq. (1) from ASCE 41–17 [32] and presented in Table A.1. The yield displacement for each story, as outlined in Table A.1, is derived from an evaluation of the displacement-step curve of each storey obtained through pushover analysis in ETABS. This yield displacement is subsequently used to conduct a nonlinear analysis of the MDOF structures in MATLAB.

Although stick models and elasto-plastic behavior offer significant computational efficiency and capture essential nonlinear characteristics for evaluating NSC demands in regular, symmetric buildings, they have limitations in capturing higher-order effects. The models may underestimate torsional effects and local deformations. Since the elasto-plastic assumption may not fully account for strain hardening, cyclic degradation, or P-delta effects, future studies should incorporate more realistic nonlinear behavior models beyond bilinear representations and explore a broader range of building case studies to strengthen the findings.

$$\delta_t = C_0 C_1 C_2 S_a \frac{T_e^2}{4\pi^2} g \tag{1}$$

In Eq. (1), C_0 represents the ratio of the roof displacement of the building to the maximum displacement of the equivalent single degree of freedom (SDOF) system, while C_1 denotes the ratio of the maximum inelastic displacements of a bilinear elastic-perfectly plastic equivalent SDOF system to the displacements calculated for the linear elastic response of the same SDOF system. C_2 accounts for the influence of pinched hysteretic shape, stiffness, and strength degradation on maximum displacement response. S_a represents the response spectrum acceleration, T_e denotes the elastic fundamental period of the bilinear approximation of the system, and g represents gravitational acceleration.

4. Description of the NSCs and their modeling assumptions

Light components with a mass less than 0.1 % of the overall mass of the supporting structures (ranging from 303 to 3211 tonnes) were considered for uncoupled analysis [64–69].

The analyzed NSCs, presented as single-degree-of-freedom systems, are categorized into three groups corresponding to the fundamental periods (T_1, T_2, and T_3) of the archetype buildings, as shown in Table 3, and are assumed to be attached at the rooftop, intermediate, and ground levels.

Aligning NSC periods with the building's fundamental modes (ranging from 0.97 s to 1.47 s) aims to maximize the seismic response amplification through resonance effects, thereby ensuring a conservative design analysis. This strategy captures realistic and frequently encountered scenarios in buildings, including tall storage rack systems [70], flexibly-mounted equipment such as medical devices, and suspended architectural or mechanical elements [71–74].

For ground-level NSCs, structural amplification effects are negligible due to direct ground motion transmission. Accordingly, the period of 0.2 s was selected based on the NBC provisions S(0.2) for the seismic analysis of NSCs. An elasto-plastic behavior model was adopted for NSCs due to its computational efficiency and ability to capture essential nonlinear characteristics. This simplification is expected to slightly overestimate the seismic response of NSCs, providing conservative results for design purposes [75,76]. Future studies should investigate more

complex hysteretic models for NSCs to better capture their actual nonlinear behavior under seismic loading. In this analysis, four ductility levels were considered: elastic (μ_{comp}=1); low ductility (μ_{comp}=1.25); moderate ductility (μ_{comp}=1.5), and high ductility (μ_{comp}=2). These ductility levels were defined as the ratio of the maximum displacement of a bilinear elastoplastic system relative to its yield displacement ($\mu_{comp} = u_m/u_y$). To implement this, the equations of motion governing the dynamic response were solved numerically at each time step using the Newmark integration method with the linear acceleration approach [42], employing parameters $\gamma = 1/2$ and $\beta = 1/6$, within a MATLAB script. This method was selected since it is widely recognized for its robustness in solving dynamic equations of motion. The equilibrium iterations were carried out to converge the displacement responses at each time increment, considering stiffness degradation and yield limits. Tangent stiffness was adjusted during the iterations to capture the changes from the linear to the nonlinear range. This approach aims to estimate the yield strength and ductility, thereby ensuring the most accurate acceleration demands possible. The discrepancies between obtained and target values of yield strength and ductility were calculated across all iterations, serving as a quantitative measure for validating the analytical accuracy.

A modal damping ratio of 5 % was adopted for all analyses. Previous investigations by Mehrjoo and Assi [77] concluded that the sensitivity of seismic demands on NSC to variations in the damping ratio is minimal, confirming the reliability and robustness of the adopted approach.

5. Fragility analyses and performance objectives of NSCs

The 24 earthquake recordings described in 2 are employed to perform nonlinear dynamic analyses. The IDA process involves scaling each record across a range of intensity levels, from 0.1 g to 4.0 g with increments of 0.1 g. This is achieved by uniformly multiplying the entire accelerogram time history by a scale factor, thereby increasing all spectral ordinates while preserving the spectral shape of the records.

Given the study's focus on acceleration-sensitive NSCs, the damage index used in the IDA is determined based on the maximum absolute acceleration demands experienced by the NSCs within the archetype structures. Then, the evaluations and extraction of fragility curves for NSCs are conducted following Hazus guidelines, with four performance levels: slight, Moderate, Extensive, and complete damage levels [41]. The fragility curve of a system represents the likelihood of exceeding a specified limit state (LS) at a given level of the seismic Intensity Measure (IM), as expressed in Eq. (2).

$$\text{Fragility} = P[\text{DM} \geq \text{LS}|\text{IM}] \tag{2}$$

Estimating the probability associated with a specific Intensity Measure (IM) value, denoted as IM = x, as expressed in Eq. (2), can be achieved by utilizing a substantial number of earthquake simulations and analyses (N_{sim}) and determining the number of occurrences that lead to exceeding the considered limit state or capacity (N_{fail}), as outlined in Eq. (3).

$$P[\text{DM} \geq \text{LS}|\text{IM} = x] \cong \frac{N_{fail}}{N_{sim}} \tag{3}$$

Typically, a log-normal function is fitted to the resulting numerical fragility data to obtain the fragility curve, as illustrated in Eq. (4).

$$P[\text{DM} \geq \text{LS}|\text{IM} = x] = \Phi\left(\frac{\ln(x/\theta)}{\beta}\right) \tag{4}$$

In the aforementioned relationship, Φ() represents the standard normal cumulative distribution function, θ denotes the mean of the fragility function, and β is the standard deviation of ln (IM = x). The lognormal distribution parameters were estimated using Maximum Likelihood Estimation (MLE), a widely adopted statistical method that optimizes probability distribution fit by maximizing the likelihood function. MLE was selected for this analysis due to its proven efficiency in parameter estimation for lognormal distributions, particularly for large datasets, as demonstrated in previous statistical studies [78,79]. Table 4 presents the specified performance levels and corresponding acceleration thresholds for acceleration-sensitive NSCs.

6. Computation of NSC seismic acceleration demands at different ductility levels

The section investigates the influence of ductility and the resonance condition on PFA (g), particularly focusing on resonance with the first three fundamental modes of the structures, when using $T_c/T_1 = 1$, $T_c/T_2 = 1$, and $T_c/T_3 = 1$. The probability of exceeding specific damage states is evaluated in terms of PFA intensity. The seismic demands on acceleration-sensitive NSCs were computed using both historical and synthetic ground motion records. Results are provided for the roof, and ground levels, as well as selected intermediate floors: level 6 in the 12-storey building, levels 4 and 5 in the 9-storey building, and level 3 in the 6-storey building.

The first subsection investigates how the attachment ductility and resonance conditions influence the fragility curves of NSCs attached to elastic structures while the second subsection focuses on the nonlinear structures. The fragility curves, shown in Figs. 5 and 6, present the probability of exceeding the specific damage states as a function of PFA intensity.

Each subplot displays 16 curves corresponding to four distinct ductility levels (μ_{comp}=1, 1.25, 1.5, 2) across the four damage states of slight, moderate, extensive, and complete. Finally, Tables 5 and 6 present the mean values of PFA (g) for a probability of exceedance of 50 % on elevated floors, alongside the average ratios of nonlinear/linear PFA (g) values. Additionally, Table 7 provides the mean values of Sa (g) for the same probability of exceedance at the ground level across the four considered damage states.

a) Fragility curves and damage states of acceleration-sensitive NSCs mounted on elastic structures

Fig. 5(a-f) presents the fragility curves for NSCs mounted on elastic structures. Subplots 5(a), 5(c), and 5(e) show responses at the roof level, while Subplots 5(b), 5(d), and 5(f) represent the responses at intermediate levels. Each subplot corresponds to resonance with the building's first three modes, specifically $T_c/T_1 = 1$, $T_c/T_2 = 1$, and $T_c/T_3 = 1$, respectively. In addition, Fig. 5 includes the ground-level responses for NSCs with a spectral period of 0.2 s.

Fig. 5(a,b) shows that the probability of exceeding a given damage state is, on average, 10 % higher at roof levels compared to intermediate levels, indicating a greater vulnerability of NSCs located at higher levels. As the resonance periods shift from T_1 in Fig. 5(a,b) to T_2 in Fig. 5(c,d), the PFA demand for a specific probability of exceeding a given damage state increases, on average, by 40 % for intermediate levels and by 11 % for roof levels. Additionally, when resonance periods shift from T_2 to T_3 (Fig. 5(e,f)), the PFA demand to exceed a damage state increases by about 50 % for both roof and intermediate levels. These trends indicate that the probability of exceeding a given damage state decreases at higher resonance periods. This is particularly noticeable at roof levels, where acceleration demand to exceed a damage state increases substantially (11–50 %), compared to intermediate levels (40–50 %).

Table 4
Peak floor accelerations used to define median values of damage to acceleration-sensitive NSCs [41].

Seismic design level	Floor acceleration at the threshold of nonstructural damage (g)			
	Slight	Moderate	Extensive	Complete
Moderate	0.25	0.50	1.00	2.00

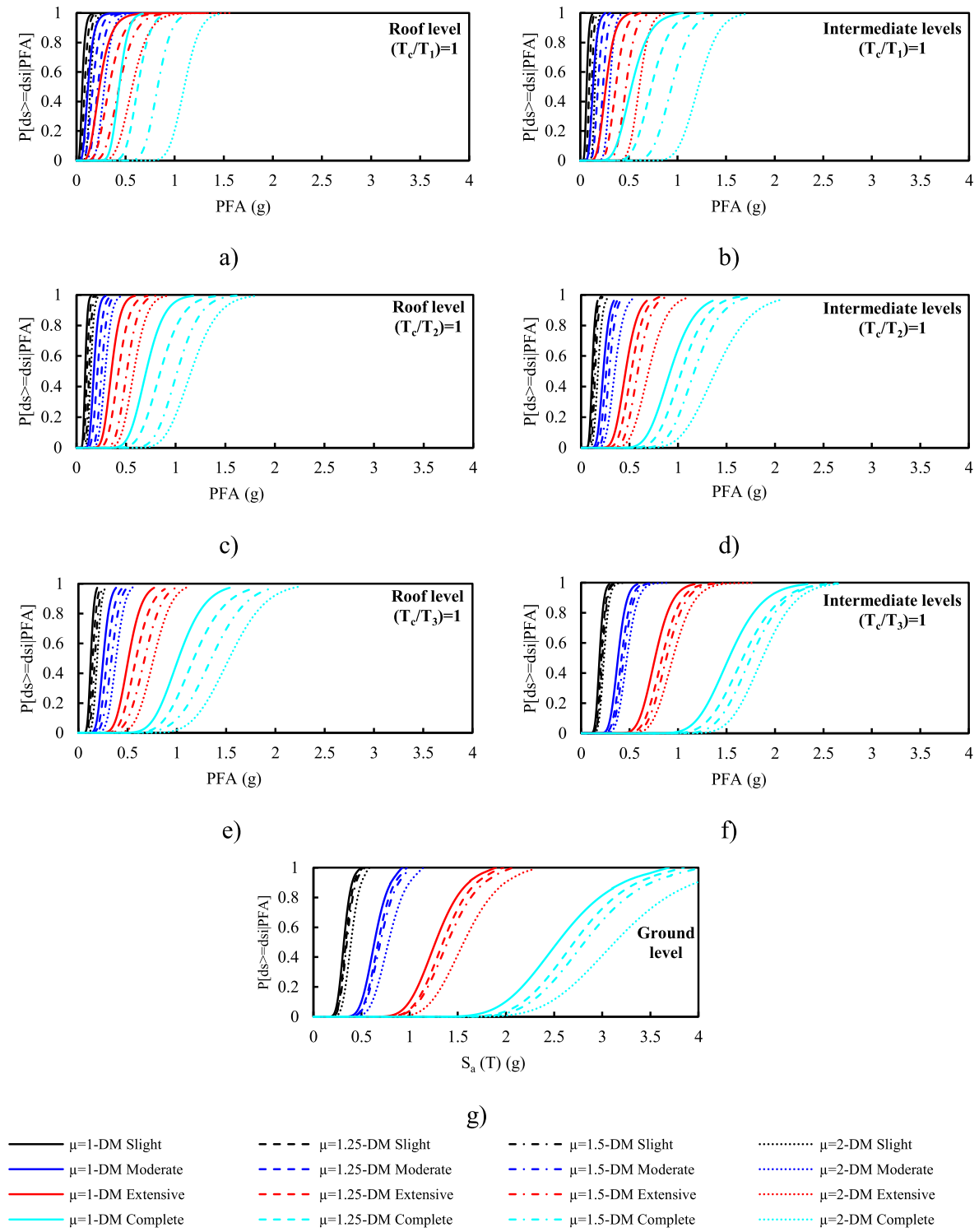

Fig. 5. Seismic fragility curves for NSCs across various ductility levels and damage states under different resonance conditions in elastic structures: a) roof level ($T_c/T_1=1$), b) intermediate level ($T_c/T_1=1$), c) roof level ($T_c/T_2=1$), d) intermediate level ($T_c/T_2=1$), e) roof level ($T_c/T_3=1$), f) intermediate level ($T_c/T_3=1$), and g) at ground level.

Comparatively, Fig. 5(g) illustrates that at ground level, the acceleration demand to exceed a damage state increases on average by 80 % compared to the T_3 resonance range and by 100 % compared to the T_2 resonance range. This further emphasizes the influence of elevation on increasing acceleration demands under seismic loading. When considering the effect of ductility levels of attachment of NSCs on their performance, Fig. 5 reveals another trend across different resonance ranges. For the T_1 resonance range at the roof level, the peak floor acceleration demand to exceed a given damage state increases on average by 144 % when moving from elastic NSCs behavior to high ductility NSCs behavior, while at the intermediate level, the average increase is 130 %. This trend is consistently observed across all damage states. For the T_2 resonance range at the roof level, the peak floor acceleration demand to exceed a given damage state increases on average by 130 % when

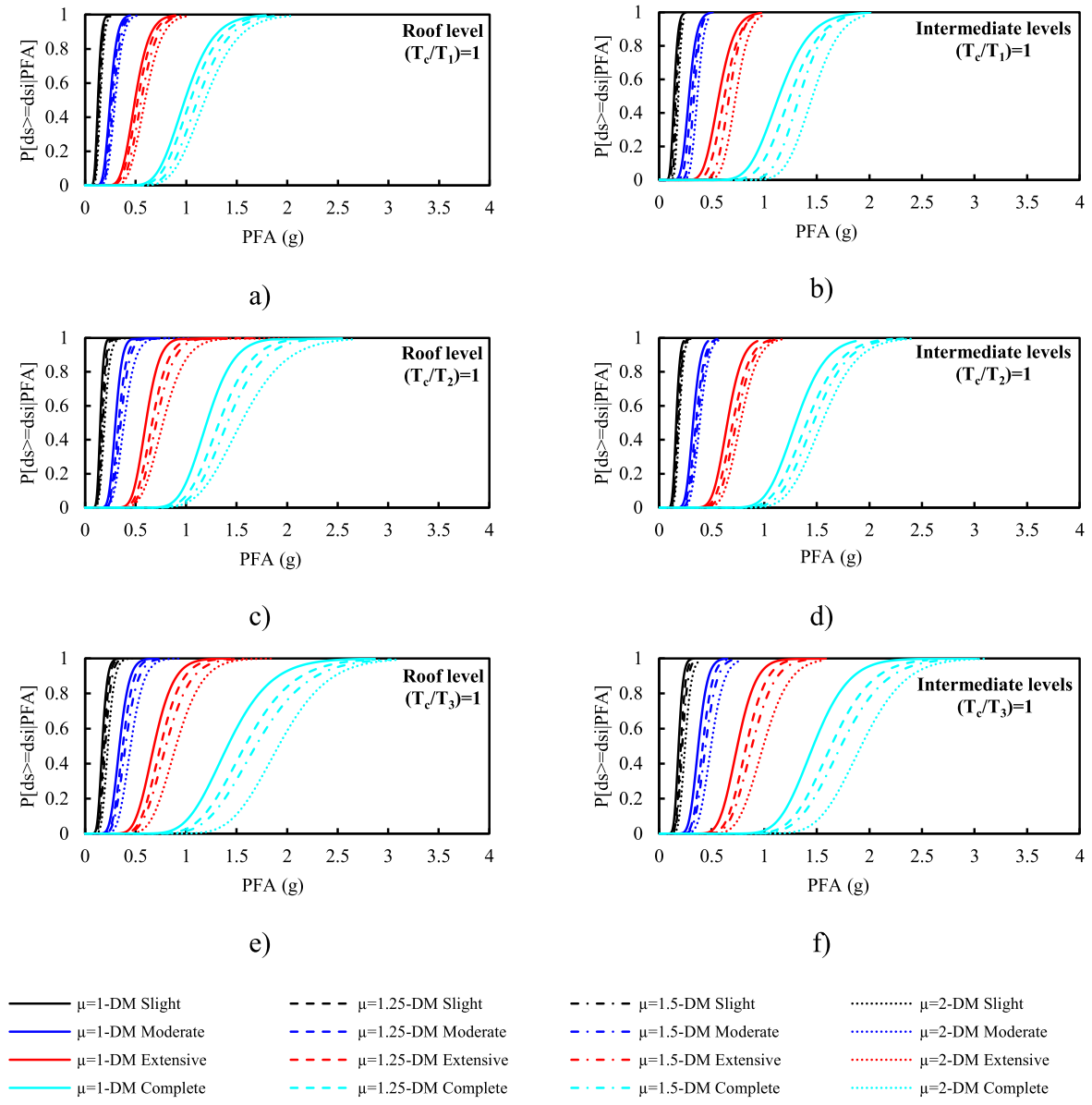

Fig. 6. Seismic fragility curves for NSCs across various ductility levels and damage states under different resonance conditions in the nonlinear structures: a) roof level (T_c/T_1=1), b) intermediate level (T_c/T_1=1), c) roof level (T_c/T_2=1), d) intermediate level (T_c/T_2=1), e) roof level (T_c/T_3=1), f) intermediate level (T_c/T_3=1).

moving from an elastic NSC behavior to a high ductility NSC behavior. On the other hand, at intermediate levels within the T_2 resonance range, peak floor acceleration demand increases by 50 % across all damage states. For the T_3 resonance range, transitioning from elastic to high ductility NSCs behavior results in more modest increases in the peak floor acceleration demand required to exceed a given damage state, averaging 50 % at the roof levels and 20 % at the intermediate levels. At ground level, transitioning from elastic to high ductility NSCs behavior leads to an average 20 % increase in spectral acceleration demand across all damage states. Overall, these findings indicate that while higher ductility levels of NSCs increase the acceleration demand required to exceed a given damage state, this effect becomes less pronounced as the resonance range shifts from T_1 to T_2 and T_3. Additionally, as observed in Fig. 5(a,b), the fragility curves of highly ductile NSCs at the slight damage state align closely with those for elastic NSCs at the moderate damage state, highlighting the beneficial impact of ductility in reducing damage likelihood under comparable seismic intensities.

This correlation also holds for the fragility curves of highly ductile NSCs in the moderate damage state, which resemble those of elastic NSCs in the extensive damage state. Furthermore, the fragility curves of highly ductile NSCs in the extensive damage state align with those of elastic NSCs in the complete damage state. The slope of fragility curves, also referred to as cumulative distribution functions (CDFs), at any specific point corresponds to the probability density function (PDF). As the probability density increases, the likelihood of a specific peak floor acceleration value triggering the respective damage state becomes higher. In this context, the fragility curves exhibit steeper slopes for the slight and moderate damage states, particularly within the T_1 and T_2 resonance ranges. Conversely, as we progress to the extensive and complete damage states, the fragility curves flatten, particularly in the T_3 resonance range and at the ground level.

In conclusion, while higher ductility levels in the attachments of NSCs enhance energy dissipation, they also increase the likelihood of potential damage to these components.

b) Fragility curves and damage states of acceleration-sensitive NSCs mounted on nonlinear structures

Table 5
Mean values of PFA (g)(T_c/T_{1-3}=1) IM at 50 % possibility of exceedance of the slight and moderate damage state (DS) in elevated floors.

			Slight DS			Moderate DS		
Resonance range (T)	**μ_{comp}**	**Specific location level**	Elastic structure	Nonlinear structure	Average nonlinear/ linear	Elastic structure	Nonlinear structure	Average nonlinear/ linear
T_1	1	Intermediate	0.066	0.143	2.16	0.13	0.29	2.16
		Roof	0.059	0.126		0.12	0.25	
	1.25	Intermediate	0.092	0.156	1.65	0.18	0.32	1.66
		Roof	0.083	0.133		0.17	0.26	
	1.5	Intermediate	0.12	0.167	1.34	0.24	0.33	1.32
		Roof	0.11	0.142		0.22	0.28	
	2	Intermediate	0.15	0.182	1.15	0.3	0.37	1.14
		Roof	0.14	0.151		0.28	0.298	
T_2	1	Intermediate	0.115	0.16	1.83	0.23	0.33	1.85
		Roof	0.066	0.15		0.132	0.3	
	1.25	Intermediate	0.13	0.176	1.6	0.26	0.35	1.57
		Roof	0.092	0.17		0.183	0.33	
	1.5	Intermediate	0.146	0.18	1.38	0.29	0.37	1.39
		Roof	0.118	0.18		0.235	0.35	
	2	Intermediate	0.174	0.19	1.17	0.35	0.39	1.2
		Roof	0.152	0.19		0.304	0.39	
T_3	1	Intermediate	0.191	0.186	1.155	0.38	0.37	1.17
		Roof	0.127	0.17		0.25	0.34	
	1.25	Intermediate	0.2	0.207	1.16	0.41	0.41	1.12
		Roof	0.146	0.187		0.3	0.37	
	1.5	Intermediate	0.22	0.22	1.09	0.44	0.44	1.14
		Roof	0.17	0.2		0.34	0.4	
	2	Intermediate	0.23	0.25	1.15	0.47	0.5	1.12
		Roof	0.19	0.23		0.38	0.45	

Table 6
Mean values of PFA (g) (T_c/ T_{1-3}=1) IM at 50 % possibility of exceedance of the extensive and complete damage state(DS) in elevated floors.

			Extensive DS			Complete DS		
Resonance range (T)	**μ_{comp}**	**Specific location level**	Elastic structure	Nonlinear structure	Average nonlinear/ linear	Elastic structure	Nonlinear structure	Average nonlinear/ linear
T_1	1	Intermediate	0.26	0.57	1.78	0.53	1.14	2.085
		Roof	0.23	0.49		0.43	0.99	
	1.25	Intermediate	0.37	0.62	1.63	0.73	1.25	1.91
		Roof	0.33	0.52		0.63	1.04	
	1.5	Intermediate	0.47	0.67	1.36	0.94	1.33	1.26
		Roof	0.43	0.56		0.83	1.11	
	2	Intermediate	0.61	0.73	1.24	1.21	1.46	1.03
		Roof	0.57	0.59		1.1	1.19	
T_2	1	Intermediate	0.46	0.65	2.03	0.92	1.3	1.79
		Roof	0.264	0.6		0.528	1.2	
	1.25	Intermediate	0.519	0.7	1.63	1.04	1.4	1.63
		Roof	0.367	0.66		0.733	1.32	
	1.5	Intermediate	0.584	0.73	1.34	1.17	1.47	1.41
		Roof	0.471	0.7		0.941	1.41	
	2	Intermediate	0.697	0.77	1.24	1.39	1.55	1.2
		Roof	0.608	0.77		1.22	1.55	
T_3	1	Intermediate	0.76	0.74	1.11	1.52	1.47	1.22
		Roof	0.51	0.68		1	1.41	
	1.25	Intermediate	0.83	0.83	1.01	1.66	1.64	1.2
		Roof	0.59	0.75		1.17	1.58	
	1.5	Intermediate	0.88	0.88	1.17	1.74	1.74	1.14
		Roof	0.68	0.8		1.35	1.69	
	2	Intermediate	0.94	0.99	1.065	1.87	1.92	1.23
		Roof	0.77	0.9		1.53	1.92	

Table 7
Mean values of Sa(g)(T) IM at 50 % possibility of exceedance of all damage state (DS) at the ground level.

μ_{comp}	**Slight DS**	**Moderate DS**	**Extensive DS**	**Complete DS**
1	0.317	0.64	1.27	2.55
1.25	0.338	0.67	1.35	2.71
1.5	0.349	0.698	1.39	2.82
2	0.39	0.78	1.56	3.13

Fig. 6(a-f) illustrates the fragility curves for NSCs mounted on nonlinear structures, showing the relationship between peak floor acceleration demand and damage states across various ductility levels and resonance periods (T_1, T_2, T_3). Ground-level NSCs are not included here, as their response is independent of the building's structural behavior and was already presented in Fig. 5(g). Subplots 6(a), 6(c), and 6(e) show responses at the roof level, while subplots 6(b), 6(d), and 6(f) represent intermediate levels corresponding to resonance with the building's first three modes.

These fragility curves show a higher probability of exceeding damage states at the roof levels than at the intermediate levels. In addition, the fragility curves for nonlinear structure in Fig. 6(a,b) show a reduced probability of exceeding damage states at the roof and intermediate levels compared to those of the elastic structure as seen in Fig. 5. This comparison emphasizes the significance of considering the actual nonlinear behavior of supporting structures in the probabilistic analysis of NSCs. The peak floor acceleration demand for a specific probability of exceeding a given damage state exhibits a distinct pattern as the system transitions from resonance periods T_1 to T_3, particularly for nonlinear structures (Fig. 6) compared to their elastic counterparts (Fig. 5). For nonlinear structures, the peak floor acceleration demand decreases by 14 % from T_1 to T_2 resonance range for intermediate floors and by 21 % for the roof. In contrast, for elastic counterparts, the decrease is more pronounced—40 % for intermediate floors and 11 % for the roof.

However, shifting from T_2 to T_3 resonance range shows a smaller increase for the peak floor acceleration demand to exceed a damage state for nonlinear structures (14 %) compared to elastic ones (50 %). This finding further confirms that the probability of exceeding damage states decreases at higher resonance periods for NSC attached to nonlinear structures.

A key observation from the fragility curves corresponding to nonlinear structures presented in Fig. 6 is that they exhibit flatter curves compared to the elastic structures shown in Fig. 5. Despite this overall flattening, the slopes of the fragility curves for the slight and moderate damage states are steeper than those for extensive and complete damage states shown in Fig. 6 for nonlinear structures. This indicates that, even in the case of nonlinear structures, there is a higher probability density associated with the peak floor acceleration values corresponding to the slight and moderate damage levels. Consequently, this suggests an increased likelihood of these NSCs reaching damage states when subjected to given peak floor accelerations. The peak floor acceleration demand required to exceed a damage state in nonlinear structures gradually increases as the NSCs shift from elastic to highly ductile. Specifically, for the T_1 resonance range, the NSCs at the roof and intermediate levels exhibit an average increase in peak floor acceleration demand to exceed a damage state by 20 % and 28 %, respectively, significantly lower than the 144 % and 130 % observed in their elastic counterpart. The T_2 resonance range follows a similar trend, with the NSCs experiencing increases in peak floor acceleration demand to exceed a damage state by an average of 16 % at the roof level and 26 % at the intermediate level, notably lower than the 130 % and 50 % increases seen in the elastic structure. In the T_3 resonance range, peak floor acceleration demand to exceed a damage state increases by an average of 35 % for NSCs at both roof and intermediate levels in the nonlinear structure, while the elastic structure saw increases of 50 % at the roof and 20 % at the intermediate level. These findings for nonlinear structures reinforce the previously observed trend in elastic structures, where increasing the ductility levels of NSCs increases peak floor acceleration demand to exceed a damage state, with this effect decreasing as the resonance range shifts from T_1 to T_2 and T_3.

c) Comparison of the mean acceleration demands for different damage states in Elastic and nonlinear Structures

To assess the impact of nonlinear structural behavior on the seismic demands of NSCs across different damage states, and how this deviates from the elastic behavior typically assumed in design codes, the mean peak floor acceleration values, PFA(g)(T), for a 50 % exceedance probability of each damage state (slight, moderate, extensive, and complete) are presented in Tables 5 and 6, derived from Figs. 5 and 6. Additionally, Tables 5 and 6 include a factor representing the average ratios of nonlinear/linear PFA (g), which quantifies the difference between linear and nonlinear structure models for each ductility level and damage state.

The results from Tables 5 and 6 indicate a trend across various ductility levels for different damage states. Specifically, as the ductility of NSCs increases, the average nonlinear/linear ratio tends to decrease for all periods within the resonance range. Notably, this trend remains consistent across all damage states, suggesting that the transition from elastic to nonlinear structural behavior has a relatively uniform impact across the resonance ranges (T_1, T_2, and T_3). This observed trend for the average nonlinear/linear ratio across all damage states is particularly pronounced in the T_1 range, where it decreases from 2.1 to 1.1 as the ductility of attachment of NSCs shifts from elastic to highly ductile. A similar trend is observed in the T_2 range, where the factor drops from 1.88 to 1.2 as the ductility of attachment of NSCs shifts from elastic to highly ductile. In the T_3 range, the decrease is less pronounced, with the average nonlinear/linear ratio dropping slightly from 1.16 to 1.14 as the ductility of attachment of NSCs shifts from elastic to highly ductile. It is worth noting that while this study mainly focuses on the influence of the first three fundamental modes (T_1, T_2, T_3), it is important to recognize that higher modes may play a more significant role in taller buildings or structures with different dynamic characteristics. Nevertheless, the observed trends in this study, such as the diminishing impact of higher modes (T_2 and T_3) compared to T_1 and the decreasing nonlinear/linear ratios at these modes, suggest that modes beyond T_3 are likely to contribute less significantly to the considered reinforced concrete building models.

Overall, low to moderate NSC ductility levels are most effective, while further increases in ductility yield minimal reductions in peak floor acceleration demands.

Moreover, the influence of ductility on the seismic demands of NSCs is more pronounced at the first fundamental resonance period and the observed impact tends to diminish for higher modes. This trend has important implications for how NSCs should be designed, particularly when considering seismic demand reduction and ductility requirements. The observed reduction in acceleration demands due to structural nonlinearity has significant implications for current code provisions. The NBC 2020 and similar international codes typically employ elastic analysis assumptions when determining NSC design forces. This assumption simplifies the complex structural response during seismic events but does not capture the potential inelastic deformations that may occur in real-world scenarios. The findings of this study demonstrate that this approach can lead to conservative design requirements, particularly for components with periods matching the structure's fundamental modes.

Analysis of the average nonlinear/linear ratios across different damage states reveals that elastic code assumptions may result in overestimation of seismic demands by factors ranging from 1.1 to 2.1 (Tables 5 and 6). This overestimation is most pronounced in the following scenarios:

- Components with periods matching T_1, where elastic assumptions overestimate demands by up to 115 % for elastic NSCs (μ_{comp}=1).
- Upper floor installations, particularly at roof levels, where the difference between elastic and nonlinear predictions is most pronounced.
- Lower ductility components, where the disparity between elastic code predictions and actual nonlinear behavior is most significant.

These overestimations can lead to over-designed and potentially more expensive NSC installations, as the design forces derived from elastic analysis are generally higher than those experienced in a nonlinear structure. However, these findings complement, rather than contradict, current code approaches by providing deeper insight into the actual behavior of designed structures under seismic loading. Similarly, to assess the impact of ductility on the seismic demands of NSCs at the ground level, across different damage states, the mean spectral acceleration values, Sa(g)(T), corresponding to a 50 % exceedance probability of a damage state (slight, moderate, extensive, and complete) are presented in Table 7. These values are derived from Fig. 5(g).

These observations further underscore the importance of considering the nonlinear behavior of buildings when evaluating the seismic demands on NSCs, as they provide a more accurate representation of the seismic force demands exerted on NSCs under varying levels of ductility and damage states.

7. Conclusion

This study provides a detailed analysis of the fragility of NSCs subjected to seismic loading, investigating the effects of ductility levels of NSC attachments and resonance period ranges (T_1, T_2, T_3) on their performance. Also, it examines the impact of the nonlinear behavior of the supporting structures on the probability of exceeding specific damage states for NSCs. The key findings of this research are summarized as follows:

- **Effect of Height:** NSCs at roof levels are significantly more vulnerable to seismic damage compared to those at intermediate or ground levels.
- **Impact of Resonance Periods:** As resonance shifts from the fundamental resonance period T_1 to higher ones (T_2, T_3), the seismic behavior of NSCs changes significantly. This shift results in reduced sensitivity to structural nonlinearity and attachment ductility, particularly in taller buildings.
- **Attachment Ductility:** While increased ductility levels reduce seismic forces, they may also increase the risk of localized damage to NSCs and their attachments. Therefore, achieving an optimal balance between ductility and acceptable damage levels is critical in NSC seismic design.
- **Structural Nonlinearity:** Accounting for the nonlinear behavior of the supporting structure is essential for improving the accuracy of probabilistic seismic assessments of NSCs. This consideration affects acceleration demands consistently across damage states and resonance ranges, simplifying seismic design provisions for NSCs.

To bridge the gap between current code provisions and the actual seismic performance of NSCs, it is essential to refine the component-specific response modification factor (*Rp*), that reflects the level of ductility of NSC attachments. Additionally, considering the nonlinear behavior of supporting structures would enhance the accuracy of seismic demand predictions.

Extending performance-based design principles to NSCs and embedding fragility-based performance objectives into building codes represents a transformative approach to improving post-earthquake functionality and resilience. This approach links damage states to ductility levels, thereby enhancing the reliability of seismic design and performance predictions and ensuring that NSCs are better equipped to withstand real-world seismic events. For acceleration-sensitive NSCs, adopting moderate ductility levels ($\mu_{comp} \approx 1.5$) provides an effective design target. This approach offers a well-balanced solution that reduces seismic demands while ensuring cost efficiency and resilience, avoiding both excessive over-design and undue risk of failure.

CRediT authorship contribution statement

Mehrjoo Majid: Writing – review & editing, Writing – original draft, Visualization, Validation, Methodology, Investigation, Formal analysis, Data curation, Conceptualization. **Assi Rola:** Writing – review & editing, Validation, Supervision, Software, Resources, Project administration, Funding acquisition, Conceptualization.

Funding information

This research was supported by the Natural Sciences and Engineering Research Council of Canada (NSERC) through the Discovery Grant RGPIN-2016–05009.

Declaration of Competing Interest

Both authors have contributed significantly to the research and preparation of the manuscript, and we have reviewed and approved the final version of the manuscript. There are no conflicts of interest among the authors.

Acknowledgments

The authors gratefully acknowledge the financial support from the Natural Sciences and Engineering Research Council of Canada (NSERC) through the Discovery Grant RGPIN-2016–05009. Special thanks to the research associate, Mr. Shahabaldin Mazloom, for carrying out the design of the case study buildings.

Appendix A. Required input and output data for the pushover analysis

Table A.1
Required input and output data for the pushover analysis

		Hinge properties used in ETABS								Output	
Case study	Target disp (m)	Hinge name	My (kN-m) +	My (kN-m) -	a	b	c	IO	LS	CP	Storey level	Yield disp(m)
3 Storey	0.72	PHB01	284.6	284.6	0.025	0.05	0.2	0.01	0.025	0.05	1st	0.05
		PHB02	227.4	266	0.025	0.05	0.2	0.01	0.025	0.05	2nd	0.071
		PHB03	222.2	222.2	0.025	0.05	0.2	0.01	0.025	0.05		
		PHB04	154.1	205.5	0.025	0.05	0.2	0.01	0.025	0.05	3rd	0.091
		PHCE01	-	-	0.038	0.078	0.2	0.005	0.039	0.05		
6 Storey	0.84	PHB01	651.5	651.5	0.02	0.03	0.2	0.005	0.02	0.03	1st	0.032
		PHB02	762.5	762.5	0.02	0.02	0.2	0.005	0.02	0.03	2nd	0.057
		PHB03	325.1	252.3	0.019	0.029	0.2	0.005	0.0193	0.029	3rd	0.098
		PHB04	250.2	176.3	0.019	0.029	0.2	0.005	0.0193	0.029	4th	0.102
		PHCE01	-	-	0.041	0.058	0.2	0.005	0.029	0.04	5th	0.122
		PHCE02	-	-	0.047	0.068	0.2	0.005	0.034	0.048	6th	0.133
9 Storey	1.5	PHB01	1076	865.6	0.01	0.015	0.2	0.0015	0.01	0.015	1st	0.036
		PHB02	1267	1190	0.01	0.015	0.2	0.0015	0.01	0.015	2nd	0.075
		PHB03	1106	997.7	0.01	0.015	0.2	0.0015	0.01	0.015	3rd	0.109

(*continued on next page*)

Table A.1 (*continued*)

Case study	Target disp (m)	Hinge properties used in ETABS								Output	
		Hinge name	My (kN-m)		a	b	c	IO	LS	CP	Storey level	Yield disp(m)
			+	-								
12 Storey	1.77	PHB04	933.1	730.3	0.01	0.015	0.2	0.0015	0.01	0.015	4th	0.125
		PHB05	690.1	455.1	0.01	0.015	0.2	0.0015	0.01	0.015	5th	0.14
		PHB06	772.4	371.7	0.02	0.03	0.2	0.005	0.2	0.03	6th	0.186
		PHB07	370.4	370.4	0.02	0.03	0.2	0.005	0.2	0.03	7th	0.202
		PHCE01	-	-	0.041	0.041	0.2	0.005	0.018	0.026	8th	0.213
		PHCE02	-	-	0.046	0.046	0.2	0.005	0.025	0.035	9th	0.22
		PHB01	1729	1441	0.01	0.015	0.2	0.0015	0.01	0.015	1st	0.016
		PHB02	2094	2033	0.01	0.015	0.2	0.0015	0.01	0.015	2nd	0.038
		PHB03	1593	1438	0.01	0.015	0.2	0.0015	0.01	0.015	3rd	0.06
		PHB04	1793	1673	0.01	0.015	0.2	0.0015	0.01	0.015	4th	0.082
		PHB05	1593	1438	0.01	0.015	0.2	0.0015	0.01	0.015	5th	0.102
		PHB06	1321	1052	0.02	0.03	0.2	0.005	0.02	0.03	6th	0.12
		PHB07	1171	885.6	0.02	0.03	0.2	0.005	0.02	0.03	7th	0.134
		PHB08	1535	1209	0.02	0.03	0.2	0.005	0.02	0.03	8th	0.145
		PHB09	656.5	754	0.02	0.03	0.2	0.005	0.02	0.03	9th	0.156
		PHB10	559.9	751.1	0.02	0.03	0.2	0.005	0.02	0.03	10th	0.164
		PHCE01	-	-	0.04	0.04	0.2	0.005	0.01	0.014	11th	0.169
		PHCE02	-	-	0.045	0.045	0.2	0.005	0.022	0.031	12th	0.173

Appendix B. Glossary of Technical Terms

- **Bilinear elastoplastic model:** A simplified representation of material behavior that combines linear elastic and perfectly plastic responses.
- **Ductility**: The ability of a material or structure to undergo plastic deformation without fracture.
- **Floor response spectra:** Graphs showing the peak response of single-degree-of-freedom systems at various natural frequencies when subjected to the motion of a specific floor in a building during an earthquake.
- **Fragility curve:** A graphical representation of the probability of exceeding a specific damage state as a function of seismic intensity.
- **Incremental Dynamic Analysis (IDA):** An advanced simulation method used to assess seismic demands across a range of earthquake intensities.
- **Non-structural components (NSCs)**: Components in a building that are not part of the main load-bearing structural system, such as mechanical equipment, partitions, and ceilings.
- **Resonance:** The dynamic amplification of system response when the excitation frequency matches or approaches the system's natural frequency, resulting in increased seismic demands on NSCs.
- **Spectral Matching**: A process to adjust or modify a signal or spectrum to match a target spectrum.
- **Uniform hazard spectrum (UHS):** A response spectrum that has an equal probability of exceedance at all periods for a given site and return period.

Data availability

Data will be made available on request.

References

[1] Toro GR, McGuire RK, Cornell CA, Sewell RT. Linear and Nonlinear Response of Structures and Equipment to California and Eastern United States Earthquakes. Electric Power Research Inst., Palo Alto, CA (USA): Risk Engineering, Inc.; 1989.

[2] Igusa T. Response characteristics of inelastic 2-DOF primary-secondary system. J Eng Mech 1990;116(5):1160–74. https://doi.org/10.1061/(ASCE)0733-9399(1990)116:5(1160).

[3] Adam C, Fotiu PA. Dynamic analysis of inelastic primary–secondary systems. Eng Struct 2000;22(1):58–71.

[4] Villaverde R. Simple method to estimate the seismic nonlinear response of nonstructural components in buildings. Eng Struct 2006;28(8):1209–21.

[5] Vukobratović V, Fajfar P. Code-oriented floor acceleration spectra for building structures. Bull Earthq Eng 2017;15(7):3013–26. https://doi.org/10.1007/s10518-016-0076-4.

[6] Applied Technology Council. NIST GCR 18-917-43(ATC). Recommendations for improved seismic performance of nonstructural components. NIST GCR 18-917-43 Natl Inst Stand Technol 2018. https://doi.org/10.6028/NIST.GCR.18-917-43.

[7] Ghasemof A, Mirtaheri M, Karami Mohammadi R. Multi-objective optimization for probabilistic performance-based design of buildings using FEMA P-58 methodology. Eng Struct 2022;254:113856. https://doi.org/10.1016/j.engstruct.2022.113856.

[8] Mehrjoo M, Aval SBB. Proposing new design and retrofitting objectives for seismic design of hospital structures: a case study of Imam Khomeini Hospital in Eslamabad-e Gharb. *Bull Earthq Eng* Publ Online June 4, 2024. https://doi.org/10.1007/s10518-024-01892-2.

[9] Obando JC, Lopez-Garcia D. Inelastic displacement ratios for nonstructural components subjected to floor accelerations. J Earthq Eng 2018;22(4):569–94. https://doi.org/10.1080/13632469.2016.1244131.

[10] Anajafi H, Medina RA, Santini-Bell E. Inelastic floor spectra for designing anchored acceleration-sensitive nonstructural components. Bull Earthq Eng 2020;18(5):2115–47.

[11] Filiatrault A, Perrone D, Merino RJ, Calvi GM. Performance-based seismic design of nonstructural building elements. J Earthq Eng 2018;25(2):237–69. https://doi.org/10.1080/13632469.2018.1512910.

[12] Kazantzi AK, Vamvatsikos D, Miranda E. Evaluation of seismic acceleration demands on building nonstructural elements. J Struct Eng 2020;146(7):04020118. https://doi.org/10.1061/(ASCE)ST.1943-541X.0002676.

[13] Banerjee AK, Pramanik D, Roy R. Seismic structural fragilities: proposals for improved methodology per spectral matching of accelerogram. Eng Struct 2016;111:538–51. https://doi.org/10.1016/j.engstruct.2016.01.002.

[14] D'Altri AM, Sarhosis V, Milani G, et al. Modeling strategies for the computational analysis of unreinforced masonry structures: review and classification. Arch Comput Methods Eng 2020;27(4):1153–85. https://doi.org/10.1007/s11831-019-09351-x.

[15] D'Ayala D., Meslem A., Vamvatsikos D., Porter K., Rossetto T. GEM Guidelines for Analytical Vulnerability Assessment of Low/Mid-Rise Buildings; 2015. doi:10.13117/GEM.VULN-MOD.TR2014.12.

[16] Roca P, Cervera M, Gariup G, Pela' L. Structural analysis of masonry historical constructions. classical and advanced approaches. Arch Comput Methods Eng 2010;17(3):299–325. https://doi.org/10.1007/s11831-010-9046-1.

[17] Nardin C, Bursi OS, Paolacci F, Pavese A, Quinci G. Experimental performance of a multi-storey braced frame structure with non-structural industrial components subjected to synthetic ground motions. Earthq Eng Struct Dyn 2022;51(9):2113–36. https://doi.org/10.1002/eqe.3656.

[18] Moon DS, Lee Y, Lee S. Seismic vulnerability assessment of RC frame structures using 3D analytical models. J Korea Acad-Ind Coop Soc 2016;17(9):724–31. https://doi.org/10.5762/kais.2016.17.9.724.

[19] Moon DS, Lee Y, Lee SM. Fragility analysis of space reinforced concrete frame structures with structural irregularity in plan. J Struct Eng 2018;144(8). https://doi.org/10.1061/(asce)st.1943-541x.0002092.

[20] Rahman A, Khan Q uz Z, Qureshi MI. Evaluation of simplified analysis procedures for a high-rise reinforced concrete core wall structure. Adv Civ Eng 2019;2019:1–21. https://doi.org/10.1155/2019/1035015.

[21] Olivo M, Bortolozzi M, Tessarolo A, Luise F. A new method for the accurate prediction of on-load power factor in two-pole induction motors considering shaft eddy currents. IEEE Trans Energy Convers 2020;35(3):1196–207. https://doi.org/10.1109/tec.2020.2976617.

[22] Anajafimarzijarani H. Improved Seismic Design of Non-Structural Components (NSCs) and Development of Innovative Control Approaches to Enhance the Seismic Performance of Buildings and NSCs. University of New Hampshire; 2018.

[23] Canadian Commission On Building And Fire Codes. National Building Code of Canada: 2020. Published online 2020. doi:10.4224/W324-HV93.

[24] Soong T.T., Chen G., Wu Z., Zhang R., Grigoriu M. Assessment of the 1991 NEHRP provisions for nonstructural components and recommended revisions. In: Assessment of the 1991 NEHRP Provisions for Nonstructural Components and Recommended Revisions. 1993:150-150.

[25] Kawakatsu T, Kitade K, Takemori T, Kuwabara Y, Ogiwara Y. Floor Response Spectra Considering Elasto-Plastic Behaviour of Nuclear Power Facilities. North-Holland Publishing Co; 1979. ⟨http://inis.iaea.org/search/search.aspx?orig_q=RN:12588757⟩.

[26] Lin J, Mahin SA. Seismic response of light subsystems on inelastic structures. J Struct Eng 1985;111(2):400–17. https://doi.org/10.1061/(ASCE)0733-9445(1985)111:2(400).

[27] Viti G, Olivieri M, Travi S. Development of non-linear floor response spectra. Nucl Eng Des 1981;64(1):33–8. https://doi.org/10.1016/0029-5493(81)90029-7.

[28] Applied Technology Council. Recommendations for Improved Seismic Performance of Nonstructural Components. National Institute of Standards and Technology; 2018. https://doi.org/10.6028/NIST.GCR.18-917-43.

[29] Kazantzi A., Vamvatsikos D., Miranda E. Effect of yielding on the seismic demands of nonstructural elements. In: Proceedings of 16th European Conference on Earthquake Engineering, Thessaloniki, Greece; 2018.

[30] Miranda E., Kazantzi A., Vamvatsikos D. Towards a New Approach to Design Acceleration-sensitive Non-structural Components; 2018.

[31] Wang T, Shang Q, Li J. Seismic force demands on acceleration-sensitive nonstructural components: a state-of-the-art review. Earthq Eng Eng Vib 2021;20(1):39–62. https://doi.org/10.1007/s11803-021-2004-0.

[32] American Society of Civil Engineers. Seismic Evaluation and Retrofit of Existing Buildings. 41st ed. American Society of Civil Engineers; 2017. https://doi.org/10.1061/9780784414859.

[33] Taghavi S., Miranda E. Probabilistic study of peak floor acceleration demands in nonlinear structures. In: Proceedings of the 15th World Conference on Earthquake Engineering (15WCEE), Lisbon, Portugal; 2012.

[34] Ruggieri S, Vukobratović V. The influence of torsion on acceleration demands in low-rise RC buildings. Bull Earthq Eng 2024;22(5):2433–68. https://doi.org/10.1007/s10518-024-01873-5.

[35] Clayton JS, Medina RA. Proposed method for probabilistic estimation of peak component acceleration demands. Earthq Spectra 2012;28(1):55–75. https://doi.org/10.1193/1.3673623.

[36] D'Angela D., Magliulo G., Zito M., Calenzo F. Seismic Fragility of Nonstructural Elements Modelled as Nonlinear Single-degree-of-freedom Systems; 2024.

[37] Gautam D, Adhikari R, Rupakhety R. Seismic fragility of structural and non-structural elements of Nepali RC buildings. Eng Struct 2021;232:111879. https://doi.org/10.1016/j.engstruct.2021.111879.

[38] Jamshidi Avanaki M. Response modification factors for seismic design of steel Fiber Reinforced Concrete segmental tunnels. Constr Build Mater 2019;211:1042–9. https://doi.org/10.1016/j.conbuildmat.2019.03.275.

[39] Abou-Elfath H, Shamel Fahmy A, Mohamed Khalifa K. Response modification factors of buckling-restrained braced frames designed according to the Egyptian code. Alex Eng J 2018;57(4):2851–64. https://doi.org/10.1016/j.aej.2018.07.001.

[40] Güner T, Topkaya C. Performance comparison of BRBFs designed using different response modification factors. Eng Struct 2020;225:111281. https://doi.org/10.1016/j.engstruct.2020.111281.

[41] FEMA 2012. Multi-Hazard Loss Estimation Methodology: HAZUS - MH 2.1 Technical Manual.

[42] Chopra AK. Dynamics of Structures. fourth ed. Pearson; 2011.

[43] Asadpour G, Asadi P, Hajirasouliha I. Analysis of bilinear hysteretic structures with nonlinear fluid viscous dampers using modified stochastic linearization technique. Eng Struct 2022;251:113555. https://doi.org/10.1016/j.engstruct.2021.113555.

[44] Hancock J, Bommer JJ, Stafford PJ. Numbers of scaled and matched accelerograms required for inelastic dynamic analyses. Earthq Eng Struct Dyn 2008;37(14):1585–607. https://doi.org/10.1002/eqe.827.

[45] American Society of Civil Engineers. Minimum Design Loads and Associated Criteria for Buildings and Other Structures. seventh ed. American Society of Civil Engineers; 2016. https://doi.org/10.1061/9780784414248.

[46] Panza G, Alvarez GF, et al. Realistic modeling of seismic input for megacities and large urban areas (the UNESCO/IUGS/IGCP project 414). Episodes 2002:25. https://doi.org/10.18814/epiiugs/2002/v25i3/002.

[47] Piscal ACM, López-Almansa F. Generating damping modification factors after artificial inputs in scenarios of local records scarcity. Bull Earthq Eng 2018;16(11):5371–96. https://doi.org/10.1007/s10518-018-0406-9.

[48] Fahjan Y., Ozdemir Z.. Scaling of Earthquake Accelerograms for Non-linear Dynamic Analyses to Match the Earthquake Design Spectra. In:; 2008. Accessed May 6, 2024. ⟨https://www.semanticscholar.org/paper/SCALING-OF-EARTHQUAKE-ACCELEROGRAMS-FOR-NON-LINEAR-Fahjan-Ozdemir/a27826c6f61009252ed97aff996b8eb1c4718469⟩.

[49] Gascot R.L., Montejo L.A. Evaluation of Spectrum Compatible Earthquake Records and Its Effect on the Inelastic Demand of Civil Structures. In:; 2014. Accessed May 6, 2024. ⟨https://www.semanticscholar.org/paper/EVALUATION-OF-SPECTRUM-COMPATIBLE-EARTHQUAKE-AND-ON-Gascot-Montejo/44f68dac585a33e69eac85e5193627b36d32c001⟩.

[50] Reyes J.C.Estimating Seismic Demands for Performance-based Engineering of Buildings. UC Berkeley; 2009. Accessed November 14, 2022https://escholarship.org/uc/item/9fp377cr.

[51] United States. Federal Emergency Management Agency, Building Seismic Safety Council (U.S.). FEMA P-1050-1, NEHRP (National Earthquake Hazards Reduction Program) Recommended Seismic Provisions for New Buildings and Other Structures. 2015 edition. FEMA; 2015. Accessed October 25, 2022. ⟨http://purl.fdlp.gov/GPO/gpo63156⟩.

[52] Chouinard L., Rosset P., De La Puente A., Madriz R., Mitchell D., Adams J. Seismic hazard analysis for Montreal. In: Proceedings of the 13th World Conference on Earthquake Engineering, Vancouver, Canada. Paper. Vol 7010.; 2004. Accessed December 11, 2024. ⟨https://www.researchgate.net/profile/Philippe-Rosset-3/publication/264886615_Seismic_hazard_analysis_for_Montreal_SEISMIC_HAZARD_ANALYSIS_FOR_MONTREAL/links/53ff724e0cf29dd7cb52137f/Seismic-hazard-analysis-for-Montreal-SEISMIC-HAZARD-ANALYSIS-FOR-MONTREAL.pdf⟩.

[53] Ghofrani H, Atkinson GM, Chouinard L, Rosset P, Tiampo KF. Scenario shakemaps for Montreal. Can J Civ Eng 2015;42(7):463–76. https://doi.org/10.1139/cjce-2014-0496.

[54] Rosset P, Chouinard LE. Characterization of site effects in Montreal, Canada. Nat Hazards 2009;48(2):295–308. https://doi.org/10.1007/s11069-008-9263-1.

[55] Atkinson G. Earthquake time histories compatible with the 2005 National building code of Canada uniform hazard spectrum. Can J Civ Eng 2009;36:991–1000. https://doi.org/10.1139/L09-044.

[56] National Research Council Canada (NRC) I f. R i. CI. National Building Code of Canada (NBCC). Published online January 1, 2015. Accessed November 14, 2021. ⟨https://nrc-publications.canada.ca/eng/view/object/?id=c8876272-9028-4358-9b42-6974ba258d99⟩.

[57] C.S.A. Group. Design of Concrete Structures (Sixth edition). Published online 2014a.

[58] Mazloom S, Assi R. Estimate of V/H spectral acceleration ratios for firm soil sites in Eastern Canada. Soil Dyn Earthq Eng 2022;159:107350. https://doi.org/10.1016/j.soildyn.2022.107350.

[59] Computers and Structures Inc. (CSI). ETABS-Building Analysis and Design. Published online 2017.

[60] Basset Salom L. The Flexibility Method. Published online May 17, 2019. Accessed July 7, 2024. ⟨https://riunet.upv.es/handle/10251/120620⟩.

[61] Georgioudakis M, Plevris V. A combined modal correlation criterion for structural damage identification with noisy modal data. Adv Civ Eng 2018:2018. https://doi.org/10.1155/2018/3183067.

[62] The MathWorks Inc. MATLAB. Published online 2023. ⟨https://www.mathworks.com/⟩.

[63] Mazloom S. Evaluation of Vertical Ground and Floor Accelerations and Spectra in Elastic RC Frame Buildings Located in Eastern Canada. phd. École de technologie supérieure; 2023. Accessed April 5, 2024. ⟨https://espace.etsmtl.ca/id/eprint/3253/⟩.

[64] Amin M., Hall W., Newmark N., Kassawara R. Earthquake Response of Multiply Connected Light Secondary Systems by Spectrum Methods; 1971:103-129.

[65] Singh A, Ang AS. Stochastic prediction of maximum seismic response of light secondary systems. Nucl Eng Des 1974;29(2):218–30.

[66] Taghavi S., Miranda E. Effect of interaction between primary and secondary systems on floor response spectra. In: 14th World Conference on Earthquake Engineering; 2008:12-17.

[67] Cunha A., Caetano E., Ribeiro P., Müller G. A critical review of current approaches on the determination of seismic force demands on nonstructural components. Published online 2014.

[68] American Society of Civil Engineers. Seismic Analysis of Safety-Related Nuclear Structures and Commentary. Published online 2000.

[69] Federal Emergancy Management Agency of United States Department of Homeland Security (DHS). PACT Beta Test Example: Building C Reinforced Masonry Shear Wall Building. FEMA P-58BD-3716. Published online 2013.

[70] Chen C.K., Scholl R.E., Blume J.A. Seismic Study of Industrial Steel Storage Racks. URS/John A. Blume and Associates, San Francisco, CA.; National Science Foundation, Washington, DC. Engineering and Applied; 1980. Accessed March 31, 2025. ⟨https://ntrl.ntis.gov/NTRL/dashboard/searchResults/titleDetail/PB81142101.xhtml⟩.

[71] Huang WC, Hussainzada N, Mcclure G. Experimental study on the seismic behaviour of suspended ceilings. Proc Annu Conf Can Soc Civ Eng 2013;2:1526–35.

[72] Setareh M. Vibration serviceability of a building floor structure. I: dynamic testing and computer modeling. J Perform Constr Facil 2010;24(6):497–507. https://doi.org/10.1061/(ASCE)CF.1943-5509.0000134.

[73] Singh MP, Moreschi LM, Suárez LE, Matheu EESeismic Design Forces. II: flexible nonstructural components. J Struct Eng 2006;132(10):1533–42. https://doi.org/10.1061/(ASCE)0733-9445(2006)132:10(1533).

[74] Magliulo G, D'Angela D. Seismic response and capacity of inelastic acceleration-sensitive nonstructural elements subjected to building floor motions. Earthq Eng Struct Dyn 2024;53(4):1421–45. https://doi.org/10.1002/eqe.4080.

[75] Oropeza M, Favez P, Lestuzzi P. Seismic response of nonstructural components in case of nonlinear structures based on floor response spectra method. Bull Earthq Eng 2010;8(2):387–400. https://doi.org/10.1007/s10518-009-9139-0.
[76] Chopra AK, Chintanapakdee C. Inelastic deformation ratios for design and evaluation of structures: single-degree-of-freedom bilinear systems. J Struct Eng 2004;130(9):1309–19. https://doi.org/10.1061/(ASCE)0733-9445(2004)130:9(1309).
[77] Mehrjoo M, Assi R. Proposed reliable peak component factors for ductile light NSCs subjected to horizontal ground motions. Published online December 11 Bull Earthq Eng 2024. https://doi.org/10.1007/s10518-024-02081-x. Published online December 11.
[78] Basak P., Basak I., Balakrishnan N. Computational Statistics and Data Analysis Estimation for the Three-parameter Lognormal Distribution Based on Progressively Censored Data. Accessed January 2, 2025. ⟨https://www.semanticscholar.org/paper/Computational-Statistics-and-Data-Analysis-for-the-Basak-Basak/d604b6c9a460d4fd3936e8bdccdac361b2f155db⟩.
[79] Cohen AC, Whitten BJ. Estimation in the three-parameter lognormal distribution. J Am Stat Assoc 1980;75(370):399–404. https://doi.org/10.2307/2287466.